



Lauretano, V., Zachos, J. C., & Lourens, L. J. (2018). Orbitally Paced Carbon and Deep-Sea Temperature Changes at the Peak of the Early Eocene Climatic Optimum. *Paleoceanography and Paleoclimatology*. <https://doi.org/10.1029/2018PA003422>

Peer reviewed version

License (if available):
Other

Link to published version (if available):
[10.1029/2018PA003422](https://doi.org/10.1029/2018PA003422)

[Link to publication record in Explore Bristol Research](#)
PDF-document

This is the accepted author manuscript (AAM). The final published version (version of record) is available online via AGU100 at <https://doi.org/10.1029/2018PA003422>. Please refer to any applicable terms of use of the publisher.

University of Bristol - Explore Bristol Research

General rights

This document is made available in accordance with publisher policies. Please cite only the published version using the reference above. Full terms of use are available: <http://www.bristol.ac.uk/red/research-policy/pure/user-guides/ebr-terms/>



Orbitally Paced Carbon and Deep-Sea Temperature Changes at the Peak of the Early Eocene Climatic Optimum

Vittoria Lauretano^{1*}, James C. Zachos², and Lucas J. Lourens¹

¹ Department of Earth Sciences, Faculty of Geosciences, Utrecht University, Princetonlaan 8a, 3584 CB Utrecht, The Netherlands.

² Earth and Planetary Sciences Dept., University of California, Santa Cruz, CA 95064, USA.

Corresponding author: Vittoria Lauretano (vittoria.lauretano@bristol.ac.uk)

* Current address: School of Chemistry, University of Bristol, Cantock's Close BS8 1TS United Kingdom

Key Points:

- Continuous record of orbitally forced hyperthermal events during the Early Eocene Climatic Optimum
- ~5.2-Myr astronomically calibrated monospecific benthic foraminiferal isotope record from the southeastern Atlantic at Walvis Ridge
- Positive shift in the benthic carbon record during the peak of the Climatic Optimum

This article has been accepted for publication and undergone full peer review but has not been through the copyediting, typesetting, pagination and proofreading process which may lead to differences between this version and the Version of Record. Please cite this article as doi: 10.1029/2018PA003422

Abstract

The late Paleocene to early Eocene warming trend was punctuated by a series of orbitally paced transient warming events, associated with the release of isotopically light carbon into the ocean-atmosphere system. These events occurred throughout the early Eocene, critically persisting during onset, peak, and termination of the Early Eocene Climatic Optimum (EECO) and the onset of the middle Eocene cooling. Here we present a ~5.2 million-year (Myr) long high-resolution benthic foraminiferal stable-isotope record spanning the peak of the early Eocene “hothouse” from Ocean Drilling Program (ODP) Leg 208 Site 1263. Our new oxygen isotope record confirms the presence of short-term warming events during the peak and termination of the EECO, previously described in coeval bulk carbonate records. The degree of change between deep-sea temperature and concurrent carbon release during these events is consistent with previous findings for Eocene Thermal Maximum (ETM) 2 to 3, suggesting that the orbitally forced processes that triggered these perturbations in the exogenic carbon pool were similar. Additionally, the long-term background carbon isotope signature reveals a rapid enrichment of up to ~1.0‰ across the peak warmth of the EECO, ~51.6 Ma, without a corresponding shift in the oxygen record suggesting a decoupling from climate. We speculate that this carbon shift reflects a non-recurrent adjustment in the mean (steady) state of the deep ocean carbon reservoir due to a significant change in carbon source/sink, the biological pump and/or ocean circulation during the extreme greenhouse conditions of the EECO.

Key words: early Eocene hyperthermals; benthic oxygen isotopes; EECO; deep-sea temperatures; Walvis Ridge, Ocean Drilling Program.

1 Introduction

The late Paleocene-early Eocene long-term warming trend reached its peak during a prolonged period of warming defined as Early Eocene Climatic Optimum (EECO; ~53-49 Ma; Kirtland Turner et al., 2014; Lauretano et al., 2015; Westerhold et al., 2018; Zachos et al., 2008, 2001). During the EECO, atmospheric CO₂ concentrations and temperatures reached by far the highest greenhouse conditions of the Cenozoic (Foster et al., 2017; Pagani et al., 2005; Zachos et al., 2008). This interval of sustained warming followed a long-term drop in $\delta^{13}\text{C}$ between 58 and 52 Ma, linked to a reduction in the flux of organic carbon burial (Komar et al., 2013), and was associated with increasing $p\text{CO}_2$ (300-1700 ppmv) (Anagnostou et al., 2016; Cui et al., 2016; Jagiecki et al., 2015).

Periodic short-lived global warming events followed the Paleocene-Eocene Thermal Maximum (PETM, ~56 Ma; e.g., Kennett and Stott, 1991; McInerney and Wing, 2011; Penman et al., 2016; Sluijs et al., 2007; Zachos et al., 2005) and persisted throughout the early Eocene and the onset of the EECO, including the ETM- 2 and 3 (Galeotti et al., 2010; Lauretano et al., 2015; Littler et al., 2014; Lourens et al., 2005; Stap et al., 2010, Westerhold et al., 2018). These hyperthermal events are associated with intense perturbations of global carbon cycle and deep-sea temperatures, recorded by intense dissolution in marine sediments and negative excursions in carbon and oxygen stable isotope records (Galeotti et al., 2017; Littler et al., 2014; Lourens et al., 2005; Sexton et al., 2011; Zachos et al., 2010). Evidence suggests that these transient events were driven by the input of vast amounts of ^{13}C -depleted carbon to the ocean-atmosphere, most likely from the destabilization of light-carbon reservoirs due to the long-term warming (Deconto et al., 2012; Dickens et al., 1997; Frieling et al., 2016; Kennett and Stott, 1991; Littler et al., 2014; Nicolo et al., 2007; Sluijs et al., 2007; Zachos et al., 2008, 2010).

Recent findings from isotope records in the equatorial Atlantic (ODP Site 1258, Demerara Rise; Kirtland Turner et al., 2014; Sexton et al., 2011) and Pacific Ocean (ODP Site 1209, Westerhold et al., 2018), spanning the early to middle Eocene, have challenged the view on the expected occurrence of hyperthermal events (i.e., increasing frequency and decreasing magnitude) during the EECO, as simulated by climate modeling based on the assumption of thermal-threshold dependency (Lunt et al., 2011). A series of $\delta^{13}\text{C}$ and $\delta^{18}\text{O}$

negative excursions of varying magnitude and frequency persisted across the EECO and into the onset of the Cenozoic cooling trend (Kirtland Turner et al., 2014; Sexton et al., 2011, 2006; Westerhold et al., 2018). However, paired $\delta^{13}\text{C}$ and $\delta^{18}\text{O}$ records across this time interval are scarce, and mainly consist of bulk stable isotope records (e.g., Site 1258, Kirtland Turner et al., 2014) and just recently a moderate-resolution ($\sim 5\text{-}10$ ky) benthic record from the equatorial Pacific (Westerhold et al., 2018). Benthic foraminiferal stable isotope data, representative of bottom-water temperature, are fundamental in assessing the degree of warming and carbon dynamics during the EECO and “hyperthermal” events (Kirtland Turner et al., 2014; Lauretano et al., 2015; Westerhold et al., 2017).

In this study, we present a $\sim 5.2\text{-Myr}$ high-resolution benthic $\delta^{18}\text{O}$ isotope record between ~ 54 and 48.8 Ma at ODP Site 1263, in the southeastern Atlantic. This monospecific *N. truempyi* benthic oxygen record complements previously published $\delta^{13}\text{C}$ data for the same site (Lauretano et al., 2016), and extends the benthic $\delta^{18}\text{O}$ isotope record (Lauretano et al., 2015) from ~ 52.4 to 48.8 Ma, providing the most detailed record (~ 4 ky) to date for this time interval. We investigate changes in deep-sea temperature and carbon cycle on long- and short- time scales, in relation to orbital forcing, to constrain magnitude and timing of these short-lived warming events and the expression of the EECO at Site 1263. We then explore the covariance of carbon and oxygen during these events and on longer time scales and compare them with other findings for the early Eocene hyperthermals Lauretano et al., 2015; Stap et al., 2010; Westerhold et al., 2018).

2 Materials and Methods

2.1 Site description and sampling

ODP Site 1263 ($28^{\circ}32'\text{S}$, $2^{\circ}47'\text{E}$) represents the shallowest site drilled during ODP Leg 208 in the southeastern Atlantic (Fig. 1). It is located below the crest of the northeast flank of Walvis Ridge, at a water depth of 2717 m, and at an estimated paleodepth of ~ 1500 m during the early Paleogene (Zachos et al., 2004). Early Paleogene sediments at Site 1263 mainly consist of calcareous nannofossils ooze, chalk and marls. Shipboard splices were obtained using magnetic susceptibility (MS) and sediment lightness (L^*) (Zachos et al., 2004).

Samples were collected at a 5-cm resolution between ~229 mcd to ~296 mcd, following the shipboard meters composite depth section (mcd) for Site 1263. The spliced interval between ~262 and ~268 mcd (from Hole A core 26H, s 2-7 in the shipboard splices) was resampled from Hole B core 22H, sections 1-5, due to scatter in the original record, without any additional stretching or squeezing of the meter composite depth scale (see Supplementary information in Lauretano et al., 2016).

2.2 Benthic stable isotopes

A total of ~1500 samples were used to generate benthic $\delta^{13}\text{C}$ (published in Lauretano et al., 2016) and $\delta^{18}\text{O}$ isotope records based on multi-specimen samples of the epifaunal (Katz et al., 2003) or probably shallow infaunal (Sexton et al., 2006) benthic foraminiferal species *Nuttalides truempyi*, picked from the $>150\ \mu\text{m}$ fraction. On average, 8 or more specimens from each sample were analyzed for stable isotopes by using a KIEL-III automated carbonate preparation device linked on-line to a Thermo-Finnigan MAT253 mass spectrometer at Utrecht University. All values are reported in standard delta notation relative to VPDB (Vienna Pee Dee Belemnite). Calibrations to the international standard (NBS-19) and to the in-house standard (Naxos) show an analytical precision of 0.03‰ and 0.08‰ for $\delta^{13}\text{C}$ and $\delta^{18}\text{O}$, respectively. Replicate measurements were performed on ~7% of the samples. Benthic data for the ETM2 (or H1/Elmo event) and H2 of Stap et al. (2010), from ~ 291 to 296 mcd, were included in this study to obtain a longer continuous record of Site 1263.

Benthic foraminiferal *N. truempyi* $\delta^{18}\text{O}$ values were corrected for seawater equilibrium adding a factor of 0.35‰ (Shackleton et al., 1987; Shackleton and Hall, 1997), assuming the disequilibrium factor to remain constant through time, prior to paleo-temperature calculations. Paleo-temperature reconstructions were obtained by applying the equation of O'Neil et al. (1969), modified by Bemis et al. (1998):

$$T\ (^{\circ}\text{C}) = 16.9 - 4.38 (\delta^{18}\text{O}_c - \delta^{18}\text{O}_{\text{sw}}) + 0.10 (\delta^{18}\text{O}_c - \delta^{18}\text{O}_{\text{sw}})^2,$$

where sea-water temperature scale was computed assuming an ice-free seawater ($\delta^{18}\text{O}_{\text{sw}}$) value of -1.2‰ (VPDB), obtained by correcting the estimated deep-sea $\delta^{18}\text{O}_{\text{sw}}$ value of -0.98‰ (SMOW) relative to PDB scales by subtracting 0.27‰ (Hut, 1987).

2.3 Time series analysis and statistical methods

Time series analysis and band-pass filtering were performed on both records in the time domain, using the most recent age model for this site by Westerhold et al. (2017).

Spectral analysis was applied to the records using the standard Blackman-Tukey method (Fig. S2) and Gaussian band-pass filtering technique (Fig. 2) as implemented in the AnalySeries software 2.0.8 (Paillard et al 1996). Prior to band-pass filtering, data were resampled at a 3-kyr resolution and detrended. Band pass filtering was centered at a frequency of 0.002469 ± 0.0008 (/kyr) for the long 405-kyr eccentricity cycle, and at 0.01 ± 0.005 for the short ~ 100 kyr eccentricity cycle.

Evolutionary wavelet spectra were obtained in the depth (Fig. S3) and time (Fig. 5) domain using the wavelet script of Torrence and Compo (<http://paos.colorado.edu/research/wavelets>), using a Morlet mother wavelet of an order of 6. Both isotope records were resampled at 3 kyrs, detrended and normalized prior to analysis.

Deming regression, an error-in-variables model accounting for errors on both x- and y- axis, as well as standard linear regression were applied to the $\delta^{13}\text{C} - \delta^{18}\text{O}$ cross plots for each hyperthermal event (Fig. 6) using RStudio (R Core Team, 2017) and the Deming package implemented in the software.

3 Early Eocene chronology

Benthic stable isotope records are plotted against age (Fig. 2), using the most recent age model by Westerhold et al. (2017). This age model is based on the integration of high-resolution X-ray fluorescence (XRF) core scanning iron intensity data, stable isotopes, bio- and magneto- stratigraphic information for the Ypresian from material from ODP Site 1258 (Leg 207, Demerara Rise), and Walvis Ridge sites (Leg 208) including Site 1263 (Westerhold et al., 2017). This new chronology reconciles the difference between radio-isotopic and astronomical ages for this time interval, resolving the “50-Ma discrepancy” present in the Geologic Time Scale (GTS2012) between these age calibrations (Vandenberghe et al., 2012; Westerhold et al., 2017). The discrepancy was caused by the questionable duration of Chron C23 in GTS2012 (Vandenberghe et al., 2012), which arises

from the short duration of magnetochron C23n.2n at Site 1258 (Suganuma and Ogg, 2006; Westerhold and Röhl, 2009; Westerhold et al., 2017).

Recently, Lauretano et al. (2016) presented two age-model options for this time interval based on the astronomical tuning of the $\delta^{13}\text{C}$ record of Site 1263 and comparison with a coeval bulk carbonate record from Site 1258. The presence of a “problematic interval” at Site 1263, characterized by a sharp $\sim 1\%$ increase in carbon values complicates a straightforward cyclostratigraphic interpretation of this record, which led to the construction of different age model options (Lauretano et al., 2016). Given the lack of evidence for a change in sedimentation rate as implied by the 3-cycle age model, the more conservative 2-cycle age model was chosen as the preferred option, consistent with the age model of Westerhold and Röhl (2009) for Site 1258. The 3-cycle age model is largely consistent with that by Westerhold et al. (2017) on the long-eccentricity scale, and the new revised chronological framework for Site 1263 confirms that the problematic interval largely coincides with Chron C23n (Westerhold et al., 2017). A longer duration of Chron C23 is also supported by new data from the early Eocene Contessa-Bottaccione sections in Italy (Galeotti et al., 2017). Comparison of this record with the $\delta^{13}\text{C}$ record of Site 1263 showed the presence of 3 rather than 2 long eccentricity cycles within C23, supporting evidence for a longer duration of this chron. Similar results are also evidenced by Turtù et al. (2017) who presented data from the newly drilled Paleocene reference section of Smirra, in the Umbria-Marche basin, showing a longer duration of Chron C23 at Smirra than indicated by the GTS2012.

The main difference between the 3-cycle age model (Lauretano et al., 2016) and the new chronology by Westerhold et al. (2017) lies in the astronomical solution chosen for the tuning process and the tuning to the short eccentricity cycle. The 3-cycle age model developed for Site 1263 (Lauretano et al., 2016) is based on tuning to the La2010d astronomical solution (Laskar et al., 2011), considered potentially the most accurate beyond 50 Ma (Westerhold et al., 2012). Westerhold et al. (2017) proposed, instead, that the La2010b orbital solution (Laskar et al., 2011) might be the most appropriate target curve. The two solutions are based on different computation of parameters and initial conditions, INPOP06 ephemeris for La2010d (Fienga et al., 2008) and INPOP08 ephemeris for La2010b (Fienga et

al., 2009). The choice of La2010b is based on evidence suggesting that this solution is consistent with the position of minima in the very long eccentricity cycle and predicts the transition from libration to circulation at ~52 Ma (Westerhold et al., 2017). Additionally, the low amplitudes of our $\delta^{13}\text{C}$ and $\delta^{18}\text{O}$ benthic records between ~53 and 53.5 Ma (Fig. 2) are in agreement with the low-amplitude modulation in eccentricity in the La2010b orbital solution, and in contrast to the high amplitude in the same interval in the La2010d solution. We refer to Westerhold et al. (2017) for an in-depth explanation on astronomically tuned age models for the early Eocene and provide the different chronologies in our supplementary material.

4 Results

4.1 Long- and short-term variability

The ~5.2 Myr-long $\delta^{13}\text{C}$ and $\delta^{18}\text{O}$ benthic records are plotted versus depth (Fig. S1), and against age (Fig. 2). The *N. truempyi* $\delta^{13}\text{C}$ record shows pronounced variability between -1‰ and +1‰ with the most positive values located in the interval between ~51-48.8 Ma. The long-term trend in $\delta^{13}\text{C}$ towards more ^{13}C -enriched values is defined by a distinct ~1.0 ‰ increase in average background values between ~51.6 and 51 Ma, modulated by the short-eccentricity cycle, which corresponds to the “problematic interval” of Lauretano et al. (2016). Background benthic $\delta^{13}\text{C}$ values following this shift remain then ~0.5 ‰ more enriched than previously in our record, with values comparable to pre-ETM2 conditions at Walvis Ridge (Stap et al., 2010, Littler et al., 2014) (Fig. 3). Comparison between our *N. truempyi* $\delta^{13}\text{C}$ record at Site 1263 with the Site 1209 reveals that Atlantic values are consistently ~0.3 ‰ heavier than at the Pacific Site, to then converge between 52 and 51.5 Ma, before diverging of about 0.2 ‰ up to the top of our record, as observed by Westerhold et al. (2018), (Fig. 4).

Benthic $\delta^{18}\text{O}$ values vary between 0 and -1.0 ‰, with several minimums as low as -1.2‰. On balance, these extremes are concentrated between ~53 and 49 Ma, which represents the warmest interval of the EECO, as constrained in low-resolution stacked benthic records (Zachos et al., 2008). Whilst the two benthic records are generally tightly coupled on the 405- and 100-kyr scales, the sharp increase in average $\delta^{13}\text{C}$ values between ~51.6 and ~51 Ma does not correspond with a concurrent feature in the $\delta^{18}\text{O}$ record, which

remains rather stable throughout our interval. Similarly as for the $\delta^{13}\text{C}$, the $\delta^{18}\text{O}$ records of Site 1263 and Site 1209 (Westerhold et al., 2018; Fig. 4) show a consistent offset of ~ 0.3 ‰ between 54 and 52 Ma, with heavier values at the Atlantic site than the Pacific. This gradient is reduced between 52 and 51.5 Ma, and greatly reduced during the hyperthermal events, to then increase slightly between 51.5 and 48.8 Ma (Fig. 4).

Our Site 1263 benthic records document at least 18 pronounced CIEs matched by coeval negative excursions in $\delta^{18}\text{O}$ (Figs. 2 and 4). The oldest of these negative excursions (~ 54 -52 Ma) correspond to well-documented early Eocene hyperthermal events, ETM2 and H2, I1, I2, J and K/X/ETM3 and L, identified in various deep-sea $\delta^{13}\text{C}$ records and land-based marine sections (Agnini et al., 2009; Cramer et al., 2003; Galeotti et al., 2010; Kirtland Turner et al., 2014; Littler et al., 2014; Lourens et al., 2005; Slotnick et al., 2012; Stap et al., 2010; Westerhold et al., 2018; Zachos et al., 2010), and described at sites 1263 and 1262 by Lauretano et al. (2015). The younger interval (~ 52 -48.8 Ma) displays 11 additional negative excursions in both benthic records, previously identified in the $\delta^{13}\text{C}$ record (Lauretano et al., 2016). The most pronounced excursions in this interval correspond to N, P and U, occurring at 51.5, 50.8 and 49.95 Ma, respectively, represented by CIEs spanning 0.7 to 0.9 ‰, and negative $\delta^{18}\text{O}$ excursions of ~ 0.5 ‰, 0.9 ‰ and 0.8 ‰, respectively. The CIEs at Site 1263 are correlated to similar transient events, initially found in the bulk carbonate isotope records at ODP Site 1258, in the equatorial Atlantic (Kirtland Turner et al., 2014; Lauretano et al., 2016), and recently described in a high-resolution benthic record at Site 1209, Shatsky Rise, in the northwestern Pacific (Westerhold et al., 2018). Our extended $\delta^{18}\text{O}$ benthic record provides evidence for the repeated occurrence of these short-lived warming events during the EECO in the southeast Atlantic. Crucially, the presence of these paired negative excursions in the benthic records at sites 1263 and 1209 corroborates the global character of these climatic and carbon cycle events.

4.2 EECO Hyperthermals: identification and characterization

The series of negative stable isotope excursions of varying magnitude observed in our records bears close similarities to the early Eocene hyperthermals (ETM-2 to -3), suggesting that these paired CIEs and $\delta^{18}\text{O}$ negative excursions may be all genetically related and can be

classified as hyperthermal events. Moreover, the benthic records at Site 1209 show evidence of paired negative excursions across the Ypresian and Lutetian, with similar characteristics to the older events identified in other marine sections (e.g., Cramer et al., 2003; Galeotti et al., 2017; Kirtland Turner et al., 2014; Lauretano et al., 2015, 2016; Littler et al., 2014; Luciani et al., 2016, 2017; Sexton et al., 2011; Slotnick et al., 2012; Westerhold et al., 2017, 2018).

One challenge is represented by the univocal identification of these fluctuations in $\delta^{13}\text{C}$ and $\delta^{18}\text{O}$ in benthic records. Kirtland Turner et al. (2014) proposed a “quantitative” criterion for the identification of hyperthermal events. They considered as potential hyperthermals those excursions more negative than the mean -1σ of the detrended records, thus avoiding choosing an arbitrary cutoff value that would disregard internal variability of independent records. To test the validity of this approach, we applied the same method to our benthic isotope records (Fig. 2). Each record was detrended by applying a Gaussian notch filter ($0 \pm 0.00025 \text{ kyr}^{-1}$) and we extracted negative peaks exceeding the mean -1σ of each detrended record. We consider as hyperthermals only excursions more negative than this threshold in both our carbon and oxygen stable isotope records (Fig. 2). This method has the advantage of introducing a reproducible criterion for isolating negative excursions from the baseline of short-term variability in our datasets. However, applying this method to records with increased scatter or different resolution, in particular $\delta^{18}\text{O}$ records, would likely result in the erroneous identification of local high-amplitude variations as hyperthermals. Although the choice of a cut-off threshold could be considered as arbitrary, this method has the advantage of offering a first-order approach for the identification of hyperthermal-like events. As suggested by the authors, it does not represent a univocal and strict way to identify hyperthermal events (Kirtland Turner et al., 2014), for which a formal definition does not exist (see Thomas et al., 2000). Ultimately, interpretations will still rely on the nature of the record, correlation to other sites, and evidence from a vast array of proxies, which highlight the need of additional high-resolution records spanning this pivotal time interval.

The events we identify at Site 1263 clearly testify strong perturbations of the carbon cycle and associated transient warming, comparable, if not in magnitude to the PETM, at least to events like ETM2 and ETM3 (Figs 2 and 3; Stap et al., 2010, Lauretano et al., 2015; Kirtland Turner et al., 2014, Littler et al., 2014, Westerhold et al., 2018). In the case of the

early Eocene hyperthermals (ETM-2 to -3), the consistent covariance between carbon and oxygen during each hyperthermal supported the hypothesis that all these events share similar characteristics (Lauretano et al., 2015; Stap et al., 2010). Assuming climate sensitivity to be constant, the relationship between changes in the carbon cycle and deep-sea warming is expressed by the slope of the regression lines of $\delta^{13}\text{C}$ versus $\delta^{18}\text{O}$ during each event, defined from its onset to recovery (Lauretano et al., 2015). Similar slopes for the early Eocene hyperthermals were interpreted as representative of similar mechanisms for the perturbation of the exogenic carbon pool scaling with warming during all the events. This interpretation relies on the assumption that carbon sequestration by the deep ocean responded linearly through time for any amount of carbon release in the exogenic carbon pool. This is consistent with the observation of the consistent scaling between CIEs in the deep ocean and in soil nodules in terrestrial settings during the early Eocene hyperthermals (Abels et al., 2016; Lauretano et al., 2015). Moreover, we consider the signal in the benthic records as representative of general deep-water conditions, in absence of possible feedbacks due to polar amplification factors, which appear to be stable and linearly scaled with temperature in an ice-free world (Cramwinckel et al., 2018).

Accordingly, we analyze the $\delta^{13}\text{C}$ and $\delta^{18}\text{O}$ covariance during the younger events in our benthic records (P to W: 50.8-49.5 Ma) (Fig. 6). Our results show that oxygen and carbon changes are linearly related during each of the events, implying that temperature changes in the deep ocean and changes in the exogenic carbon are consistently coupled, as observed for the older hyperthermals (Lauretano et al., 2015). We apply both linear regression and Deming regression to our datasets of each hyperthermal (Fig. 6). Deming regression accounts for error in the data on both the x- and y- axis, therefore allowing to assess the relative relationship between carbon and oxygen without assigning an independent (i.e., temperature) and a dependent (i.e., carbon release) variable.

The slopes of the regression lines fall in similar range as found for the older events, with values comprised between 0.5 and 0.7 for both linear and Deming regression (see Figs. 6 and 7 in Lauretano et al. 2015), with the exception of R, for which Deming regression shows a slope of 0.9, although the slope of the linear regression is coherent with the results from the

other events. Our findings support the hypothesis that during all these events, changes in the carbon cycle and temperature response are consistently related.

A similar approach has been used to investigate the relationship between carbon and oxygen for the hyperthermals at Site 1209 (Westerhold et al., 2018). In that case, the events PETM, ETM2, ETM3, P, S, T and C21nH1 (the last younger than our record), are found to show a lower -i.e. less steep- slope than the other events, suggesting a relative larger contribution of a lighter, possibly methane-related, source of carbon for these events. Moreover, the position of these events with respect to eccentricity (at the rising of a limb in long eccentricity) and their temporal spacing are used as additional evidence for the link between these events and a slow-recharged methane carbon source (Westerhold et al., 2018). Our results at Site 1263 (Fig. 6) show that all events fall within variability of the slope of the regression lines (0.5-0.7), indicating a consistent mechanism between carbon change and warming for all the events. This method mainly provides a qualitative assessment of the relationship between carbon change and scaled warming and can be influenced by the number of data points available for each event (Lauretano et al., 2015) as well as other influences on global carbon cycle mass balance and sensitivity of T to greenhouse forcing. Clearly, more records across this interval are necessary to discriminate different sources between events, as our results at Site 1263 do not show such distinctive differences as observed at Site 1209.

4.3 Orbital forcing

Spectral and wavelet analyses (Figs. S2, S3 and 5) of the $\delta^{13}\text{C}$ and $\delta^{18}\text{O}$ benthic records confirm that power is concentrated at long- and short- eccentricity bands, with distinct peaks at 405, 125 and 95 kyr in both records, in accordance with findings from other records, including magnetic susceptibility, color reflectance, Fe- intensity and stable isotope records for the early Paleogene (Littler et al., 2014; Lourens et al., 2005; Westerhold et al., 2017, 2018; Zachos et al., 2010). Power spectra of both records yield only a very weak, if present, signal in the precession and obliquity frequency bands. This feature could be, however, a consequence of the low sedimentation rate at Site 1263, which ranges between 1.75 to 1.1 cm kyr^{-1} across Chron C23 (Westerhold et al., 2017).

Wavelet analysis was performed on both detrended and normalized records after removal of >0.6 Myr periodicities, to obtain a clearer picture of the eccentricity, obliquity and precession terms, by using a Gaussian notch filter and normalizing (Fig. 5). The long (405-kyr) eccentricity cycle represents the strongest and most stable signal across both records, as already observed over much of the upper Paleocene and early Eocene (Littler et al., 2014; Kirtland Turner et al., 2014, Lauretano et al., 2015; Westerhold and Röhl, 2009; Westerhold et al., 2017, 2018; Zachos et al., 2010). The short (~ 125 and 95 kyr) eccentricity cycles show higher spectral power in correspondence with the most pronounced short-term events in both isotope records (Fig. 5).

5 Discussion

5.1 The EECO at Site 1263

The long-term rise in temperature associated with the EECO is represented in our data by a decrease in background $\delta^{18}\text{O}$ benthic values of ~ 0.5 ‰ between 53 and 50 Ma, corresponding with an increase in bottom water temperatures of $\sim 2^\circ\text{C}$, in the absence of ice-volume effects (Figs. 2 and 4). Based on our paleotemperature calibrations, mean deep-sea temperature rose from $\sim 12^\circ\text{C}$ prior to ETM2 (Stap et al., 2010) to an average of $\sim 14^\circ\text{C}$ during the EECO and persisted through most of our record (Figs. 2 and 3). At Site 1263, the general decrease of ~ 0.3 ‰ in $\delta^{13}\text{C}$ and $\delta^{18}\text{O}$ around 53.2 Ma, coincident with the occurrence of J event, was suggested to represent the onset of the EECO (Lauretano et al. 2015). This event is also coincident with the transition from limestones to marls at Mead Stream, interpreted to represent the effect of an enhanced hydrological cycle in response to increase warming (Slotnick et al., 2012). Following this decrease, temperature continued to rise to at least ~ 49.5 Ma in our record. The highest temperatures are found in an interval of ~ 2 Myr, from 52 to 49.5 Ma, when average deep-water temperature at Site 1263 reached their maximum values of 14.0 - 15°C . A definition of the EECO is however difficult to establish without comparison to multiple sites. Based on comparison between Pacific (Site 1209) and the Atlantic sites,

Westerhold et al. (2018) suggest that the EECO can be defined between 53.2 Ma, consistent with its onset at the J event, and 49.140 Ma, corresponding with the C22nH5 event close to the top of C22n, at the onset of the cooling trend. This would lead to a total duration for the EECO of ~ 4.12 Myr (Westerhold et al., 2018). This definition is supported by our benthic records at Site 1263, showing that the highest temperature at this site were reached across a similar temporal window. However, due to drilling disturbance at Site 1263 across C22n (Lauretano et al., 2016, Westerhold et al., 2017), it is difficult to determine the termination of the EECO linked to C22nH5, as this hyperthermal is not present in our record (Fig. 4).

The negative carbon and oxygen isotope excursions that persist across the peak of the EECO do not appear to decrease in size, as also observed at Site 1258 (Kirtland Turner et al., 2014) and Site 1209 (Westerhold et al., 2018). Their magnitudes are often similar to those of the better-known early Eocene hyperthermals (i.e., ETM-2 to -3; Lauretano et al., 2015, Littler et al., 2014; Stap et al., 2010). In this regard, the younger events P (50.8 Ma) and U (49.9 Ma) are associated with a temperature increase on the order of 1.2 °C to 2.5 °C above background values, which is comparable to that of ETM2 and H2 (Stap et al., 2010). These observations raise implications for the dynamics of carbon release associated with these events. Assuming a model in which the release of carbon from an isotopically light source is dependent on the existence of a thermodynamic threshold, the gradual depletion of this source at the peak of the EECO is expected to lead to events of increased frequency and decrease magnitude (Kirtland Turner et al., 20014; Lunt et al., 2011). At Site 1263, these events continued to occur with variable magnitude as well as frequency, suggesting that additional mechanisms and/or sources could have been involved in the carbon release dynamics for these younger hyperthermals.

5.2 Hyperthermals and orbital forcing

The stable covariance of our benthic carbon and oxygen isotopes during each of the short-term events represented at Site 1263 suggests that similar drivers of change in the carbon cycle and deep-sea temperature were operating for both the early Eocene (ETM2 to -3) and the events during the EECO. On average, slope values for the younger events are steeper than showed for the early Eocene hyperthermals, and closer to the values identified in

the case of H2 and I2 (> 0.6), but all fall within the variability observed for the slopes of all events (0.5-0.7). For H2 and I2 events, in theory steeper slopes indicate a relatively greater contribution from an isotopically heavier (i.e., less ^{13}C -depleted) source of carbon with respect to a lighter, possibly methane-derived, carbon reservoir (Lauretano et al., 2015). If this hypothesis holds, the steeper slopes observed for these later hyperthermals might suggest, as in the case of I2 and H2, a relatively larger contribution of isotopically heavier sources, i.e. organic carbon ($\delta^{13}\text{C} \cong -25 \text{‰}$). This observation could be reconciled with the redistribution of dissolved organic carbon as the main mechanism for the late early to middle Eocene events (Sexton et al., 2011). In this view, the cessation of the long-term temperature rise would have halted the destabilization of isotopically light carbon reservoirs, most likely methane clathrate deposits (or permafrost carbon), which require longer recharge times, while high temperatures allowed for the redistribution of the dissolved organic carbon from the surface reservoirs to the deep ocean. At Site 1209, PETM, ETM-2 and -3, P, S, T and C21nH1 show “less steep” slopes that could testify a relatively lighter source of carbon, namely from a methane source, as hypothesized in the case of the PETM (Dickens et al., 1997; Westerhold et al., 2018). Our results at Site 1263 for the events from P to W (Fig. 6) do not show significant differences between slopes to confidently support this hypothesis and discriminate between events. However, if the slopes for these younger Eocene events implicate a heavier source of carbon (i.e., organic carbon), this suggests that the carbon excursions could represent the response to orbitally driven climatic processes involving the ocean-atmosphere system, as simulated by Zeebe et al. (2017).

Orbital forcing appears to be the main pacer for these events, in particular long- and short- eccentricity cycles (Figs. 2 and 5). The direct influence of orbital forcing was initially postulated for these transient events in the stable isotope carbon record of composite marine records (Cramer et al., 2003). The warming we observe in the $\delta^{18}\text{O}$ at our site, also supported by the Pacific benthic record at Site 1209 (Westerhold et al., 2018) (Fig. 4), points to a strong coupling between orbitally paced changes in the carbon cycle and global temperature response. Towards the peak and termination of the EECO, the frequency of these short-lived events at Site 1263 intensifies, leading to the occurrence of more closely spaced events on short-eccentricity frequencies (Fig. 2). This suggests an enhanced sensitivity to orbital

forcing in this time interval, with additional carbon release or redistribution of dissolved organic carbon occurring with almost each short-eccentricity maximum, across the warmest interval of the EECO. This observation is consistent with the increase in frequency of dissolution events recorded in the Umbria-Marche basin (Galeotti et al., 2017), suggesting that at the peak of the extreme climatic condition of the EECO, carbon release was triggered with each eccentricity cycle. In the view of a thermodynamic threshold being crossed during enhanced warming conditions, the relative timing required for the recharge of an isotopically light, likely methane-related, carbon reservoir would not be reconciled with the increased frequency of the younger hyperthermals. We therefore suggest that multiple sources/mechanisms, rather than one finite reservoir of light carbon, were likely involved in the carbon releases that characterize this time interval, maintaining that a methane-related source could still be plausible for the larger events (Westerhold et al., 2018).

The $\delta^{18}\text{O}$ record shows a weak imprint of a 41-kyr cycle, which sporadically exceeds the 95% confidence limit, Fig. 5). Obliquity is absent in the deeper benthic isotope and coarse fraction records at Site 1262 from the late Paleocene to the early Eocene where the precession signal is strong (~53–61 Ma; Littler et al., 2014) and very poorly expressed at Site 1263. Still, an obliquity forcing has been proposed by models that link hyperthermal events to the release of soil carbon from permafrost at high latitudes (DeConto et al., 2012). The large reservoirs of permafrost soil carbon on Antarctica during the early Paleogene may have contributed to carbon release during phases of high obliquity and high eccentricity. This hypothesis is based on early Eocene land-based sections from the Umbria–Marche basin, which record a ~1.2-Myr obliquity-related modulation during the early Eocene hyperthermal events (Galeotti et al., 2010). However, low sedimentation rate and bioturbation can bias the cycle signal, for example by merging two precession cycles (~40 kyr) and producing an apparent obliquity signal. This could be the case of Site 1263, for which detailed observations of core scanning proxies reveal the presence of eccentricity-modulated precession cycles rather than obliquity cycles (Westerhold et al., 2017). Moreover, experiments with using a long-term ocean-atmosphere-sediment carbon cycle reservoir model (LOSCAR; Zeebe et al., 2012) demonstrate that eccentricity modulation of precession on the carbon cycle-climate system can easily explain the observations. This presumes increased carbon burial during eccentricity

minima, with a more equable climate, increased long-term burial of organic carbon (in terrestrial reservoirs), thus resulting in a lighter exogenic carbon reservoir during eccentricity maxima (Zeebe et al., 2017). In these simulations, a high-latitude obliquity forcing is not required to explain the changes observed cycle pattern of $\delta^{13}\text{C}$ and $\delta^{18}\text{O}$ for the Paleocene-Eocene (Zeebe et al., 2017).

5.3 Coupled Cycles and Decoupled Trends

Our ~5.2 Myr- long $\delta^{13}\text{C}$ and $\delta^{18}\text{O}$ benthic records provide new constraints on the relationship between the long-term temperature rise and perturbations in the carbon cycle that characterized the early Eocene. The strong coherence between carbon and the oxygen records on long- and short- eccentricity time scales indicates that the strong coupling between climate and carbon cycle in the eccentricity bands persisted throughout the early Paleogene, as simulated by carbon cycle models (Littler et al., 2014; Lourens et al., 2005; Westerhold et al., 2017; Zachos et al., 2010; Zeebe et al., 2016, 2018). Cross-spectral analysis of the $\delta^{13}\text{C}$ and $\delta^{18}\text{O}$ benthic records reveals high coherence at all eccentricity-controlled orbital frequencies suggesting that global carbon cycle and climate were closely coupled on orbital timescales (Fig. S4). Cross-spectral phase estimates over the entire record show that changes in benthic $\delta^{18}\text{O}$, representative of bottom water temperatures, lead $\delta^{13}\text{C}$ by ~22 (± 12) kyr on the 405- eccentricity cycle and ~5 (± 2) kyr on the short-eccentricity cycle. These results are in agreement with similar findings in the Eocene at Site 1262 (Littler et al., 2014).

Changes in global climate and associated response in the carbon cycle during the EECO are therefore orbitally paced and, as a result of our tuning approach, are assumed to occur in phase with changes in the long eccentricity band. During eccentricity maxima, warming in deep/intermediate waters triggered the release of ^{13}C -depleted carbon in the ocean-atmosphere system, which led to further greenhouse warming as a positive feedback (Lauretano et al., 2016; Ma et al. 2011, Westerhold et al. 2015). However, the high coherence and overall in-phase behavior between $\delta^{13}\text{C}$ and $\delta^{18}\text{O}$ on short- and long- eccentricity time scales, in combination with a short response time, prevents precise resolution of the relative timing of the initial warming and the enhanced temperature increase due to the carbon release. This coupled behavior is reflected in the concurrent negative excursions in the $\delta^{13}\text{C}$

and $\delta^{18}\text{O}$ during our hyperthermal events as well as in the orbitally modulated background conditions in between the events.

An unusual feature in our records is the positive shift in mean $\delta^{13}\text{C}$ values of $\sim+1$ ‰ between ~ 51.6 and 51 Ma (Lauretano et al., 2016). Mean background $\delta^{18}\text{O}$ values, in contrast, remain constant within background variability during this time interval, consistent with stable and sustained high temperatures at the peak of the EECO (Fig. 2). To better characterize these long-term trends, we extracted the periodicities longer than 600 kyrs in the $\delta^{13}\text{C}$ and $\delta^{18}\text{O}$ records (Fig. 7). The clear decoupling between the two records from ~ 51.6 Ma represents a deviation from the standard pattern of the system for the late Paleocene and early Eocene, when decreases in $\delta^{13}\text{C}$ generally covary with decreases in $\delta^{18}\text{O}$, and vice versa. The stability in ~ 1 ‰ ^{13}C -enriched background values after the shift suggests that this feature represents a new state of the system, at least for the ~ 2 -Myr interval to the top of our record. In this regard, the positive excursion in $\delta^{13}\text{C}$ is a long-lasting signature in the isotope record rather than a transient event, bearing closer similarities to the Miocene Monterey excursion (Holbourn et al., 2007) than, for example, to the positive excursions associated to OAEs in the Cretaceous (Jenkyns, 2010).

A similar shift is also observed in the bulk carbonate record at Site 1258 (Kirtland Turner et al., 2014), although less pronounced, in the bulk $\delta^{13}\text{C}$ of Tethyan sections (Luciani et al., 2017), as well as in the benthic record at Site 1209 (Westerhold et al., 2018), where it is constrained to between 51.2 and 51 Ma (Fig. 4). This demonstrates that this signal is representative of the global ocean carbon reservoir. If so, several mechanisms could contribute to the observed increase in $\delta^{13}\text{C}$ values. For example, processes involving changes in carbon fluxes consistent with the removal of isotopically light carbon through increase carbonate or organic matter burial (Fisher and Arthur 1977; Faul and Delaney, 2010; Komar and Zeebe, 2016, 2011; Kump and Arthur, 1999). This can be achieved with an increase in marine phytoplankton productivity or increased preservation of organic matter under anoxic conditions, as changes in rates of organic carbon burial are linearly reflected in the isotopic composition of the carbonate fraction (Kump and Arthur, 1999). A parallel for this shift can be drawn with the Paleocene Carbon Isotope Maximum (PCIM; ~ 58.1 Ma; Littler et al., 2014). This positive peak in the late Paleocene happened, however, on faster time scales (<

100 kyr) and it has been linked to burial of organic matter, possibly in the southwest Pacific (Hollis et al., 2014; Littler et al., 2014). The hypothesis of high rates of organic carbon burial fluxes during the early Eocene is supported by evidence of a highly efficient biological pump at least until ~ 53 Ma, reflected in strong $\delta^{13}\text{C}$ surface to deep oceanic gradients (Hilting et al., 2008). Moreover, the application of paleoproductivity proxies (i.e. carbonate, silica, biogenic barium and phosphorus MARs) to early Eocene sediments from the Southern Ocean shows that export productivity and organic carbon burial fluxes peaked in the South Atlantic during the early Eocene (ODP Sites 689/690 Maud Rise; Faul and Delaney, 2010), as also evidenced in shifts in Tl and S curves between ~45 and ~55 Ma (Kurtz et al., 2003; Nielsen et al., 2009). Increased rates of organic carbon burial fluxes, in turn, should serve as a negative feedback for atmospheric $p\text{CO}_2$ withdrawal causing climate cooling. The expected cooling, however, is not represented in the $\delta^{18}\text{O}$ record. Instead, global temperatures remained consistently high throughout the EECO at Site 1263, as well as Site 1209 (Fig. 4). In addition, despite large discrepancies in estimates from different proxies, early Eocene $[\text{CO}_2]_{\text{atm}}$ remained at high levels during the EECO, with upper limit estimates of 1400-1800 ppm (Hyland and Sheldon, 2013), most likely ≥ 1000 ppm (at a 95% confidence interval; Anagnostou et al., 2016), or, as recently proposed, 1260 ppm based on estimates from nahcolite proxies (Jagniecki et al., 2015).

Therefore, we question whether this signal in our benthic carbon record might reflect a change in the isotopic composition of an end-member of the carbon source or sink, without involving a concomitant change in carbon fluxes. These mechanisms could be consistent with a change through time in the relative composition of organic matter, i.e. terrestrial vs. marine organic carbon burial (Hilting et al., 2008, Zeebe et al., 2017). Alternatively, other mechanisms could invoke changes in carbon isotope fractionation relative to the local source of carbon (Sluijs and Dickens, 2012).

Westerhold et al. (2018) also propose a change in the mean isotopic composition of the carbon source or sink to explain the +0.75 ‰ shift in $\delta^{13}\text{C}$ at Site 1209. They propose that the timing of this shift is consistent with a phase of global reorganization of the plate-mantle system, changes in seafloor spreading rates, and chaotic diffusion of planetary orbits identified in the transition from libration to circulation (Westerhold et al., 2017; 2018). A

reduced CO₂ degassing, linked to a decrease in ocean-crust production, would have led to less ¹²C-enriched carbon emissions, shifting the average isotopic composition of the δ¹³C to heavier values (Westerhold et al., 2018). However, this hypothesis is still difficult to reconcile with the unchanged levels of high pCO₂ and other phenomena must be accounted for to balance the system.

While the causes of the shift are difficult to disentangle, the high-amplitude variability in δ¹³C preceding the shift and the conditions following it suggest that the ocean-atmosphere system underwent fundamental instability before crossing into a new steady state. Our records validate findings at Site 1209 (Westerhold et al., 2018) and confirm that this change in the carbon cycle and the stable deep-ocean temperatures were a global feature. Additional data and modeling efforts should be employed to shed light on the possible causes.

Conclusions

We presented high-resolution orbitally tuned carbon and oxygen stable isotope records spanning the early Eocene between ~54 and 48.8 Ma from the ETM2 to the onset of the cooling phase, providing a complete high-resolution paired benthic foraminiferal record across the EECO in the South Atlantic. Our results confirm the presence of multiple events of global warming across the peak warming and termination of the EECO. Their varying magnitude and frequency contradict the theoretical model involving a thermal threshold for the progressive depletion of a finite light-carbon reservoir (Lunt et al., 2011). We compared δ¹³C and δ¹⁸O covariance during these events showing a consistent linear relationship between carbon release and temperature increase, as observed for the older hyperthermal events. Our hypothesis is that multiple sources/mechanisms are responsible for the carbon release associated with these events, possibly involving more ¹³C-enriched sources of carbon, as well as light methane-derived reservoirs. The short-eccentricity pacing of the youngest warming events suggests that sensitivity to orbital forcing intensifies during the warming peak of the EECO, linking carbon release to the crossing of a climatic threshold during each short-eccentricity maximum. While tightly coupled on short-term scales, carbon and oxygen trends appear decoupled on longer term scales. The gradual increase of ~1‰ in average δ¹³C values from ~ 51.6 to 51 Ma is associated to a stable record of sustained high temperatures in

the oxygen benthic record, suggesting that changes in carbon fluxes did not have a direct impact on temperatures during the EECO, confirming the global nature of this shift, also observed in the Pacific Site 1209 (Westerhold et al., 2018).

Acknowledgments, Samples, and Data

This research was funded by NWO-ALW grant (project number 865.10.001) to L.J. Lourens. We are grateful to the International Ocean Discovery Program (IODP) for providing the samples used in this study. We thank A. van Dijk and D. Kasjaniuk at Utrecht University for analytical support and F. Hilgen for useful discussions. We are thankful to the Editor and two anonymous referees whose comments greatly improved the manuscript.

The data presented in this paper are available in the Supporting Information and archived in the PANGAEA database.

References

- Abels, H. A., Lauretano, V., van Yperen, A., Hopman, T., Zachos, J. C, Lourens, L. J., Gingerich, P. D., Bowen, G.J., 2016. Carbon isotope excursions in paleosol carbonate marking five early Eocene hyperthermals in the Bighorn Basin, Wyoming. *Climate of the Past*, 12, 1–13 www.clim-past.net/12/1/2016/doi:10.5194/cp-12-1-2016.
- Agnini, C., Macri, P., Backman, J., Brinkhuis, H., Fornaciari, E., Giusberti, L., Luciani, V., Rio, D., Sluijs, A., Speranza, F., 2009. An early Eocene carbon cycle perturbation at ~52.5 Ma in the Southern Alps: Chronology and biotic response. *Paleoceanography* 24. <https://doi.org/10.1029/2008PA001649>
- Anagnostou, E., John, E.H., Edgar, K.M., Foster, G.L., Ridgwell, A., Inglis, G.N., Pancost, R.D., Lunt, D.J., Pearson, P.N., 2016. Changing atmospheric CO₂ concentration was the primary driver of early Cenozoic climate. <https://doi.org/10.1038/nature17423>

Cramer, B.S., Wright, J.D., Kent, D. V., Aubry, M.-P., 2003. Orbital climate forcing of $\delta^{13}\text{C}$ excursions in the late Paleocene-early Eocene (chrons C24n-C25n).

Paleoceanography 18,. <https://doi.org/10.1029/2003PA000909>

Cramwinckel, M. J., Huber, M., Kochen, I. J., Agnini, C., Bijl, P.K., Bohaty, S.M., Frieling, J., Goldner, A., Hilgen, F. J., Kip, E. J., Peterse, F., van der Ploeg, R., Röhl, U., Schouten, S., Sluijs, A., 2018. Synchronous tropical and polar temperature evolution in the Eocene. Nature, doi.org/10.1038/s41586-018-0272-2

DeConto, R.M., Galeotti, S., Pagani, M., Tracy, D., Schaefer, K., Zhang, T., Pollard, D., Beerling, D.J., 2012. Past extreme warming events linked to massive carbon release from thawing permafrost. Nature 484, 87–91. <https://doi.org/10.1038/nature10929>

Dickens, G.R., Neil, J.R.O., Rea, D.K., Owen, R.M., 1995. Dissociation of oceanic methane hydrate as a cause of the carbon isotope excursion at the end of the Paleocene. Paleoceanography 10, 965–971.

Dickens, G.R., Castillo, M.M., Walker, J.C.G., 1997. A blast of gas in the latest Paleocene: Simulating first-order effects of massive dissociation of oceanic methane hydrate.

Geology 25, 259.Faul, K.L., Delaney, M.L., 2010. A comparison of early Paleogene export productivity and organic carbon burial flux for Maud Rise, Weddell Sea, and Kerguelen Plateau, south Indian Ocean. Paleoceanography 25, PA3214.

<https://doi.org/10.1029/2009PA001916>

Fienga, A., Manche, H., Laskar, J., and Gastineau, M., 2008. INPOP06: a new numerical planetary ephemeris, Astron. Astrophys., 477, 315–327, <https://doi.org/10.1051/0004-6361:20066607>.

Fienga, A., Laskar, J., Morley, T., Manche, H., Kuchynka, P., Le Poncin-Lafitte, C., Budnik, F., Gastineau, M., and Somenzi, L., 2009. INPOP08, a 4-D planetary ephemeris: from asteroid and time-scale computations to ESA Mars Express and Venus Express

contributions, *Astron. Astrophys.*, 507, 1675–1686, <https://doi.org/10.1051/0004-6361/200911755>.

Foster, G.L., D.L. Royer, and D.J. Lunt, 2017. Future climate forcing potentially without precedent in the last 420 million years. *Nature Communications*, 8: p. 14845.

Frieling, J., Svensen, H.H., Planke, S., Cramwinckel, M.J., Selnes, H., Sluijs, A., 2016. Thermogenic methane release as a cause for the long duration of the PETM. *Proc. Natl. Acad. Sci. U. S. A.* 113, 12059–12064. <https://doi.org/10.1073/pnas.1603348113>

Galeotti, S., Krishnan, S., Pagani, M., Lanci, L., Gaudio, A., Zachos, J.C., Monechi, S., Morelli, G., Lourens, L.J., 2010. Orbital chronology of Early Eocene hyperthermals from the Contessa Road section, central Italy. *Earth Planet. Sci. Lett.* 290, 192–200. <https://doi.org/10.1016/j.epsl.2009.12.021>

Galeotti, S., Moretti, M., Sabatino, N., Sprovieri, M., Ceccatelli, M., Francescone, F., Lanci, L., Lauretano, V., Monechi, S., 2017. Cyclochronology of the Early Eocene carbon isotope record from a composite Contessa Road-Bottaccione section (Gubbio, central Italy). *Newsletters Stratigr.* 50, 231–244. <https://doi.org/10.1127/nos/2017/0347>

Hilting, A.K., Kump, L., Bralower, T.J., 2008. Variations in the oceanic vertical carbon isotope gradient and their implications for the Paleocene-Eocene biological pump. *Paleoceanography* 23. <https://doi.org/10.1029/2007PA001458>

Hollis, C.J., Tayler, M.J.S., Andrew, B., Taylor, K.W., Lurcock, P., Bijl, P.K., Kulhanek, D.K., Crouch, E.M., Nelson, C.S., Pancost, R.D., Huber, M., Wilson, G.S., Ventura, G.T., Crampton, J.S., Schiøler, P., Phillips, A., 2014. Organic-rich sedimentation in the South Pacific Ocean associated with Late Paleocene climatic cooling. *Earth-Science Rev.* 134, 81–97. <https://doi.org/10.1016/J.EARSCIREV.2014.03.006>

Holbourn, A.E., Kuhnt, W., Schulz, M., Flores, J.A., and Andersen, N., 2007. Middle Miocene long-term climate evolution: Eccentricity modulation of the “Monterey”

carbon-isotope excursion: *Earth and Planetary Science Letters*, v. 261, p. 534–550,
doi:10.1016/j.epsl.2007.07.026

Hyland, E.G., Sheldon, N.D., 2013. Coupled CO₂-climate response during the Early Eocene Climatic Optimum. *Palaeogeogr. Palaeoclimatol. Palaeoecol.* 369, 125–135.
<https://doi.org/10.1016/j.palaeo.2012.10.011>

Jagniecki, E.A., Lowenstein, T.K., Jenkins, D.M., Demicco, R. V., 2015. Eocene atmospheric CO₂ from the nahcolite proxy. *Geology* 43, G36886.1.
<https://doi.org/10.1130/G36886.1>

Jenkyns, H. C. (2010), Geochemistry of oceanic anoxic events, *Geochem. Geophys. Geosyst.*, 11, Q03004, doi:10.1029/2009GC002788.

Katz, M.E., 2003. Early Cenozoic benthic foraminiferal isotopes: Species reliability and interspecies correction factors. *Paleoceanography* 18, 1–12.
<https://doi.org/10.1029/2002PA000798>

Kennett, J.P., Stott, L.D., 1991. Abrupt deep-sea warming, paleoceanographic changes and benthic extinctions at the end of the Palaeocene. *Nature* 353, 225–228.
<https://doi.org/10.1038/350055a0>

Kirtland Turner, S., Sexton, P., Charles, C.D., Norris, R.D., 2014. Persistence of carbon release events through the peak of early Eocene global warmth. *Nat. Geosci.* 12, 1–17.
<https://doi.org/10.1038/ngeo2240>

Komar, N., Zeebe, R.E., 2011. Oceanic calcium changes from enhanced weathering during the Paleocene-Eocene thermal maximum: No effect on calcium-based proxies. *Paleoceanography* 26. <https://doi.org/10.1029/2010PA001979>

Komar, N., Zeebe, R.E., 2016. Calcium and calcium isotope changes during carbon cycle perturbations at the end-Permian. *Paleoceanography* 31, 115–130.
<https://doi.org/10.1002/2015PA002834>

Kump, L., Arthur, M. a., 1999. Interpreting carbon-isotope excursions: carbonates and organic matter. *Chem. Geol.* 161, 181–198. [https://doi.org/10.1016/S0009-2541\(99\)00086-8](https://doi.org/10.1016/S0009-2541(99)00086-8)

Kurtz, A. C., Kump, L., Arthur, M. A., Zachos, J.C., Paytan, A., 2003. Early Cenozoic decoupling of the global carbon and sulfur cycles. *Paleoceanography* 18. <https://doi.org/10.1029/2003PA000908>

Laskar, J., Fienga, a., Gastineau, M., Manche, H., 2011. La2010: A new orbital solution for the long term motion of the Earth 4, 17.

Lauretano, V., Littler, K., Polling, M., Zachos, J.C., Lourens, L.J., 2015. Frequency, magnitude and character of hyperthermal events at the onset of the Early Eocene Climatic Optimum. *Clim. Past* 11, 1313–1324. <https://doi.org/10.5194/cp-11-1313-2015>

Lauretano, V., Hilgen, F.J., Zachos, J.C., Lourens, L.J., 2016. Astronomically tuned age model for the early Eocene carbon isotope events: A new high-resolution $\delta^{13}\text{C}_{\text{benthic}}$ record of ODP Site 1263 between ~ 49 and ~ 54 Ma. *Newsletters Stratigr.* 49, 383–400. <https://doi.org/10.1127/nos/2016/0077>

Littler, K., Röhl, U., Westerhold, T., Zachos, J.C., 2014. A high-resolution benthic stable-isotope record for the South Atlantic: Implications for orbital-scale changes in Late Paleocene-Early Eocene climate and carbon cycling. *Earth Planet. Sci. Lett.* 401, 18–30. <https://doi.org/10.1016/j.epsl.2014.05.054>

Lourens, L.J., Sluijs, A., Kroon, D., Zachos, J.C., Thomas, E., Röhl, U., Bowles, J., Raffi, I., 2005. Astronomical pacing of late Palaeocene to early Eocene global warming events. *Nature* 435, 1083–1087. <https://doi.org/10.1038/nature03814>

Luciani, V., Dickens, G., Backman, J., Fornaciari, E., Giusberti, L., Agnini, C., D’Onofrio, R., 2016. Major perturbations in the global carbon cycle and photosymbiont-bearing

planktic foraminifera during the early Eocene. *Climate of the Past*, 12(4), 981–1007.
<https://doi.org/10.5194/cp-12-981-2016>

Luciani, V., D'Onofrio, R., Dickens, G. R., Wade, B. S., 2017. Planktic foraminiferal response to early Eocene carbon cycle perturbations in the southeast Atlantic Ocean (ODP Site 1263). *Global and Planetary Change*, 158(Supplement C), 119–133.
<https://doi.org/10.1016/j.gloplacha.2017.09.007>

Lunt, D.J., Ridgwell, A., Sluijs, A., Zachos, J.C., Hunter, S., Haywood, A., 2011. A model for orbital pacing of methane hydrate destabilization during the Palaeogene A series of transient global warming events. <https://doi.org/10.1038/NGEO1266>

McCarren, H., Thomas, E., Hasegawa, T., Röhl, U., Zachos, J.C., 2008. Depth dependency of the Paleocene–Eocene carbon isotope excursion: paired benthic and terrestrial biomarker records (Ocean Drilling Program Leg 208, Walvis Ridge). *Geochem. Geophys. Geosyst.* 9, Q10008. <http://dx.doi.org/10.1029/2008GC002116>.

McInerney, F. a., Wing, S.L., 2011. The Paleocene-Eocene Thermal Maximum: A Perturbation of Carbon Cycle, Climate, and Biosphere with Implications for the Future. *Annu. Rev. Earth Planet. Sci.* 39, 489–516. <https://doi.org/10.1146/annurev-earth-040610-133431>

Nicolo, M.J., Dickens, G.R., Hollis, C.J., Zachos, J.C., 2007. Multiple early Eocene hyperthermals: Their sedimentary expression on the New Zealand continental margin and in the deep sea. *Geology* 35, 699. <https://doi.org/10.1130/G23648A.1>

Nielsen, S.G., Mar-Gerrison, S., Gannoun, A., LaRowe, D., Klemm, V., Halliday, A.N., Burton, K.W., Hein, J.R., 2009. Thallium isotope evidence for a permanent increase in marine organic carbon export in the early Eocene. *Earth Planet. Sci. Lett.* 278, 297–307. <https://doi.org/10.1016/j.epsl.2008.12.010>

Pagani, M., Zachos, J.C., Freeman, K.H., Tipple, B., Bohaty, S., 2005. Marked Decline in Atmospheric Carbon Dioxide Concentrations During the Paleogene 600–603.

- Penman, D.E., Kirtland Turner, S., Sexton, P., Norris, R.D., Dickson, A.J., Boulila, S., Ridgwell, A., Zeebe, R.E., Zachos, J.C., Cameron, A., Westerhold, T., Röhl, U., 2016. An abyssal carbonate compensation depth overshoot in the aftermath of the Palaeocene–Eocene Thermal Maximum. *Nat. Publ. Gr.* 9. <https://doi.org/10.1038/NGEO2757>
- Sexton, P.F., Wilson, P. a., Norris, R.D., 2006. Testing the Cenozoic multisite composite $\delta^{18}\text{O}$ and $\delta^{13}\text{C}$ curves: New monospecific Eocene records from a single locality, Demerara Rise (Ocean Drilling Program Leg 207). *Paleoceanography* 21, PA2019. <https://doi.org/10.1029/2005PA001253>
- Sexton, P.F., Norris, R.D., Wilson, P. a., Pälike, H., Westerhold, T., Röhl, U., Bolton, C.T., Gibbs, S.J., 2011. Eocene global warming events driven by ventilation of oceanic dissolved organic carbon. *Nature* 471, 349–352. <https://doi.org/10.1038/nature09826>
- Slotnick, B.S., Dickens, G.R., Nicolo, M.J., Hollis, C.J., Crampton, J.S., Zachos, J.C., Sluijs, A., 2012. Large-Amplitude Variations in Carbon Cycling and Terrestrial Weathering during the Latest Paleocene and Earliest Eocene: The Record at Mead Stream, New Zealand. *J. Geol.* 120, 487–505. <https://doi.org/10.1086/666743>
- Sluijs, A., Brinkhuis, H., Schouten, S., Bohaty, S.M., John, C.M., Zachos, J.C., Reichart, G.-J., Sinninghe Damsté, J.S., Crouch, E.M., Dickens, G.R., 2007. Environmental precursors to rapid light carbon injection at the Palaeocene/Eocene boundary. *Nature* 450, 1218–21. <https://doi.org/10.1038/nature06400>
- Sluijs, A., Dickens, G.R., 2012. Assessing offsets between the $\delta^{13}\text{C}$ of sedimentary components and the global exogenic carbon pool across early Paleogene carbon cycle perturbations. *Global Biogeochem. Cycles* 26. <https://doi.org/10.1029/2011GB004224>
- Stap, L., Lourens, L.J., Thomas, E., Sluijs, A., Bohaty, S., Zachos, J.C., 2010. High-resolution deep-sea carbon and oxygen isotope records of Eocene Thermal Maximum 2 and H2. *Geology* 38, 607–610. <https://doi.org/10.1130/G30777.1>

Suganuma, Y., Ogg, J. G., 2006. Campanian through Eocene magnetostratigraphy of Sites 1257–1261, ODP leg 207, Demerara Rise (western equatorial Atlantic). *Proceedings of the Ocean Drilling Program, Scientific Results, Volume 207*

Thomas, E., Shackleton, N.J., 1996. The Paleocene-Eocene benthic foraminiferal extinction and stable isotope anomalies. *Geol. Soc. London, Spec. Publ.* 101, 401–441.
<https://doi.org/10.1144/GSL.SP.1996.101.01.20>

Thomas, E., J.C. Zachos, and T. J. Bralower, 2000, Deep-Sea Environments in the Absence of Polar Ice Caps: The Case of The Early Eocene. *In Warm Climates in Earth History*, B.T. Huber, K.G. MacLeod, S.L. Wing (Eds.), Cambridge Univ. Press, p.132-160

Turtù, A., Lauretano, V., Catanzariti, R., Hilgen, F.J., Galeotti, S., Lanci, L., Moretti, M., Lourens, L.J., 2017. Integrated stratigraphy of the Smirra Core (Umbria-Marche Basin, Apennines, Italy): A new early Paleogene reference section and implications for the geologic time scale. *Palaeogeogr. Palaeoclimatol. Palaeoecol.* 487.
<https://doi.org/10.1016/j.palaeo.2017.08.031>

Vandenbergh, N., Hilgen, F. J., Speijer, R. P., Ogg, J. G., Gradstein, F. M., Hammer, O., Hollis, C. J., and Hooker, J. J., 2012. Chapter 28 –The Paleogene Period, in: *The Geologic Time Scale*, edited by Gradstein, F. M., Ogg, J. G., Schmitz, M. D., and Ogg, G. M., Elsevier, Boston, 855–921, <https://doi.org/10.1016/B978-0-444-59425-9.00028-7>.

Westerhold, T., Röhl, U., Laskar, J., Raffi, I., Bowles, J., Lourens, L.J., Zachos, J.C., 2007. On the duration of magnetochrons C24r and C25n and the timing of early Eocene global warming events: Implications from the Ocean Drilling Program Leg 208 Walvis Ridge depth transect. *Paleoceanography* 22.
<https://doi.org/10.1029/2006PA001322>

Westerhold, T., Röhl, U., Raffi, I., Fornaciari, E., Monechi, S., Reale, V., Bowles, J., Evans, H.F., 2008. Astronomical calibration of the Paleocene time. *Palaeogeogr.*

Palaeoclimatol. Palaeoecol. 257, 377–403.

<https://doi.org/10.1016/j.palaeo.2007.09.016>

Westerhold, T., Röhl, U., 2009. High resolution cyclostratigraphy of the early Eocene – new insights into the origin of the Cenozoic cooling trend. *Clim. Past* 5, 309–327.

<https://doi.org/10.5194/cp-5-309-2009>

Westerhold, T., Röhl, U., Laskar, J., 2012. Time scale controversy: Accurate orbital calibration of the early Paleogene. *Geochemistry, Geophys. Geosystems* 13.

<https://doi.org/10.1029/2012GC004096>

Westerhold, T., Röhl, U., Frederichs, T., Bohaty, S.M., Zachos, J.C., 2015. Astronomical calibration of the geological timescale: closing the middle Eocene gap. *Clim. Past* 11, 1181–1195.

<https://doi.org/10.5194/cp-11-1181-2015>

Westerhold, T., Röhl, U., Frederichs, T., Agnini, C., Raffi, I., Zachos, J.C., Wilkens, R.H., 2017. Astronomical calibration of the Ypresian timescale: implications for seafloor spreading rates and the chaotic behavior of the solar system? *Clim. Past* 13, 1129–

1152. <https://doi.org/10.5194/cp-13-1129-2017>

Westerhold, T., Röhl, U., Donner, B., Zachos, J. C., 2018. Global Extent of Early Eocene Hyperthermal Events – a new Pacific Benthic Foraminiferal Isotope Record from Shatsky Rise (ODP Site 1209). *Paleoceanography and Paleoclimatology*. doi:

10.1029/2017PA003306

Zachos, J.C., Pagani, M., Sloan, L., Thomas, E., Billups, K., 2001. Trends, rhythms, and aberrations in global climate 65 Ma to present. *Science* 292, 686–693.

Zachos, J.C., Röhl, U., Schellenberg, S.A., Sluijs, A., Hodell, D.A., Kelly, D.C., Thomas, E., Nicolo, M., Raffi, I., Lourens, L.J., McCarren, H., Kroon, D., 2005. Rapid

acidification of the ocean during the Paleocene-Eocene thermal maximum. *Science* 308, 1611–5. <https://doi.org/10.1126/science.1109004>

Zachos, J.C., Dickens, G.R., Zeebe, R.E., 2008. An early Cenozoic perspective on greenhouse warming and carbon-cycle dynamics. *Nature* 451, 279–283.

<https://doi.org/10.1038/nature06588>

Zachos, J.C., McCarren, H., Murphy, B., Röhl, U., Westerhold, T., 2010. Tempo and scale of late Paleocene and early Eocene carbon isotope cycles: Implications for the origin of hyperthermals. *Earth Planet. Sci. Lett.* 299, 242–249.

<https://doi.org/10.1016/j.epsl.2010.09.004>

Zeebe, R. E. 2012. LOSCAR: Long-term ocean-atmosphere-sediment Carbon cycle Reservoir Model v2.0.4. *Geoscientific Model Development*, 5(1), 149–166.

<https://doi.org/10.5194/gmd-5-149-2012>Zeebe2012, R.E., Ridgwell, A., Zachos, J.C.,

2016. Anthropogenic carbon release rate unprecedented during the past 66 million years. *Nat. Geosci.* 9, 325–329. <https://doi.org/10.1038/ngeo2681>

Zeebe, R. E., Westerhold, T., Littler, K., & Zachos, J. C., 2017. Orbital forcing of the Paleocene and Eocene carbon cycle. *Paleoceanography*, 32, 440–465.

<https://doi.org/10.1002/2016PA003054><https://doi.org/10.1002/2016PA003054>



Figure 1. Paleogeographic reconstruction for the early Eocene (~55 Ma) showing the position of ODP Sites 1263 (generated at www.odsn.de/odsn/services/paleomap/paleomap.html).

Accepted

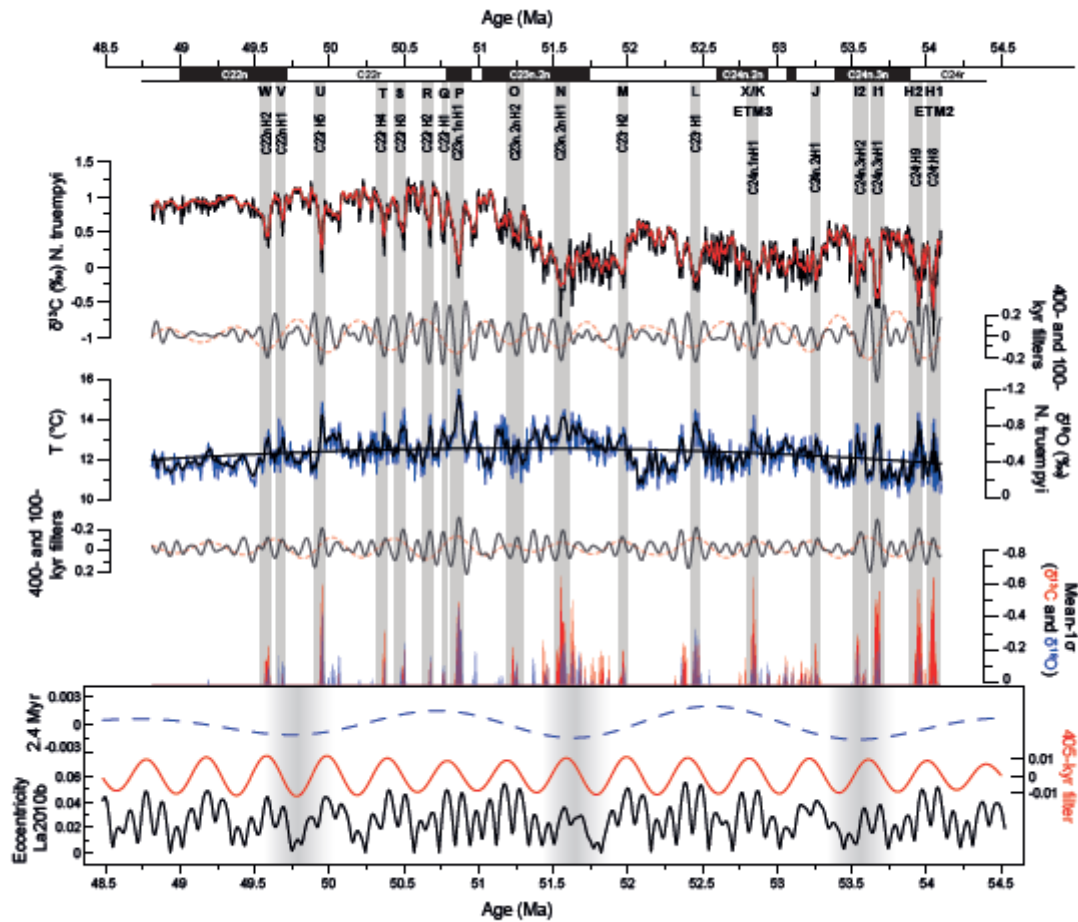


Figure 2. Benthic *N. truempyi* $\delta^{13}\text{C}$ and $\delta^{18}\text{O}$ records of Site 1263 plotted versus age (Westerhold et al., 2017), and band-pass filtering of the long- and short- eccentricity cycle for both records. The plotted $\delta^{18}\text{O}$ benthic record represents raw data, while it was corrected for paleotemperature calculations (see methods). Magnetostratigraphic information from the framework for the Walvis Ridge Sites from Westerhold et al. (2017). The identification of the hyperthermals is determined by excursions exceeding mean - 1σ (Kirtland Turner et al., 2014, see text). Labels for the events from Westerhold et al. (2018), based on magnetostratigraphic information, and Lauretano et al. (2016), continuing the alpha-numeric scheme of Cramer et al. (2003). Eccentricity components of the La2010b orbital solution (Laskar et al., 2011).

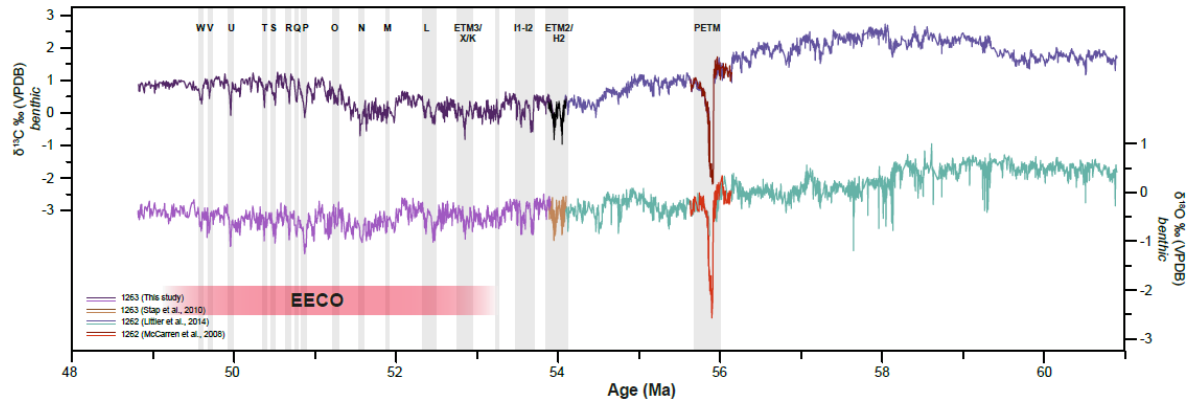


Figure 3. Composite records of benthic $\delta^{13}\text{C}$ and $\delta^{18}\text{O}$ for the late Paleocene-early Eocene at Walvis Ridge. Data from sites 1262 (Littler et al., 2014; McCarren et al., 2008; Stap et al., 2010) and 1263 (this study; Lauretano et al., 2015, 2016; Stap et al., 2010). Age model from Westerhold et al., 2017.

Accepted Article

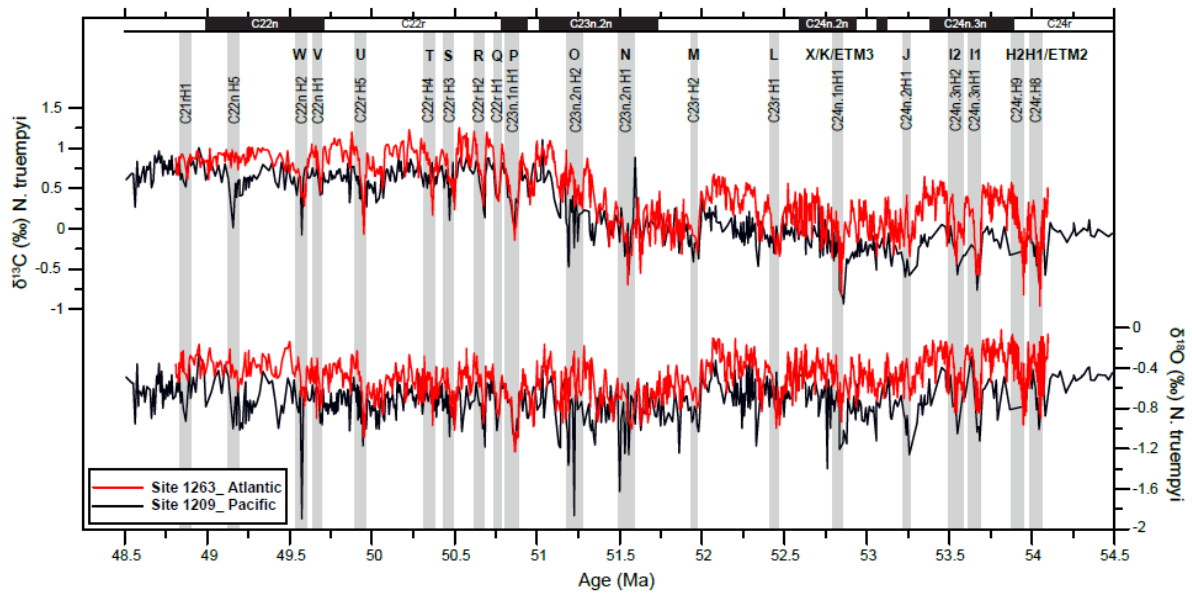


Figure 4. *N. truempyi* $\delta^{13}\text{C}$ and $\delta^{18}\text{O}$ records of Site 1263 and Site 1209 (Westerhold et al., 2018). Magnetostratigraphic information from the Walvis Ridge Sites from Westerhold et al. (2017). Grey bars indicate the position of hyperthermal events.

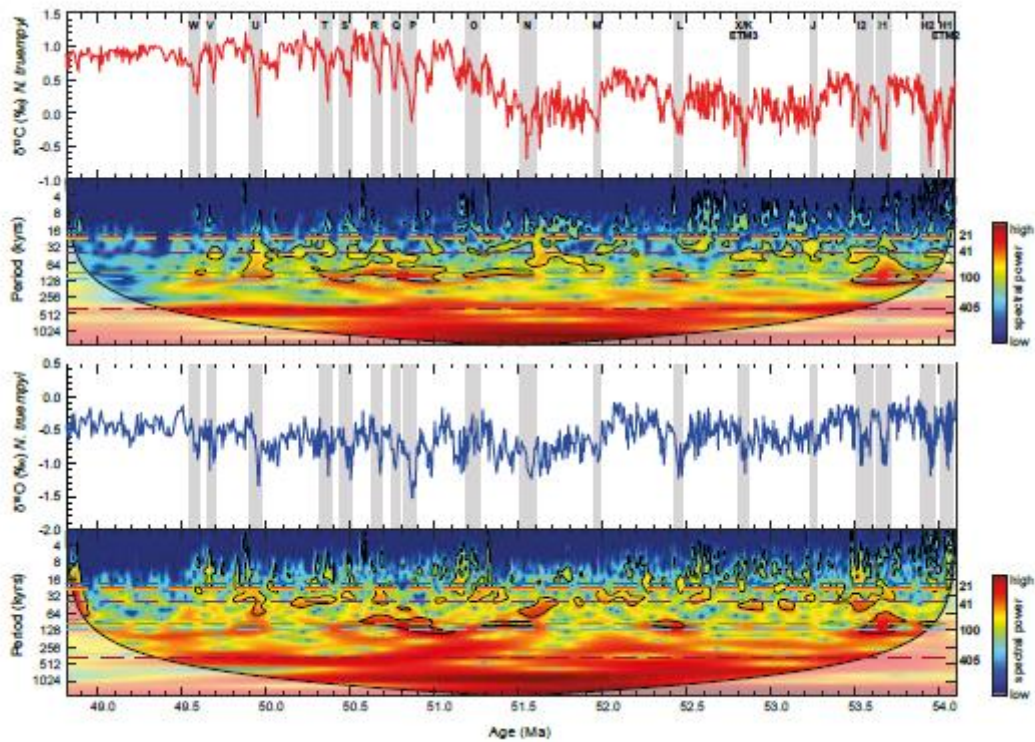


Figure 5. Evolutionary wavelet analyses for $\delta^{13}\text{C}$ and $\delta^{18}\text{O}$ were performed using a Morlet mother wavelet with an order of 6. The shaded area represents the 95% significance level. Spectral power above the confidence level is concentrated at distinct frequencies, corresponding to the long 405-kyr and short eccentricity 100-kyr cycles.

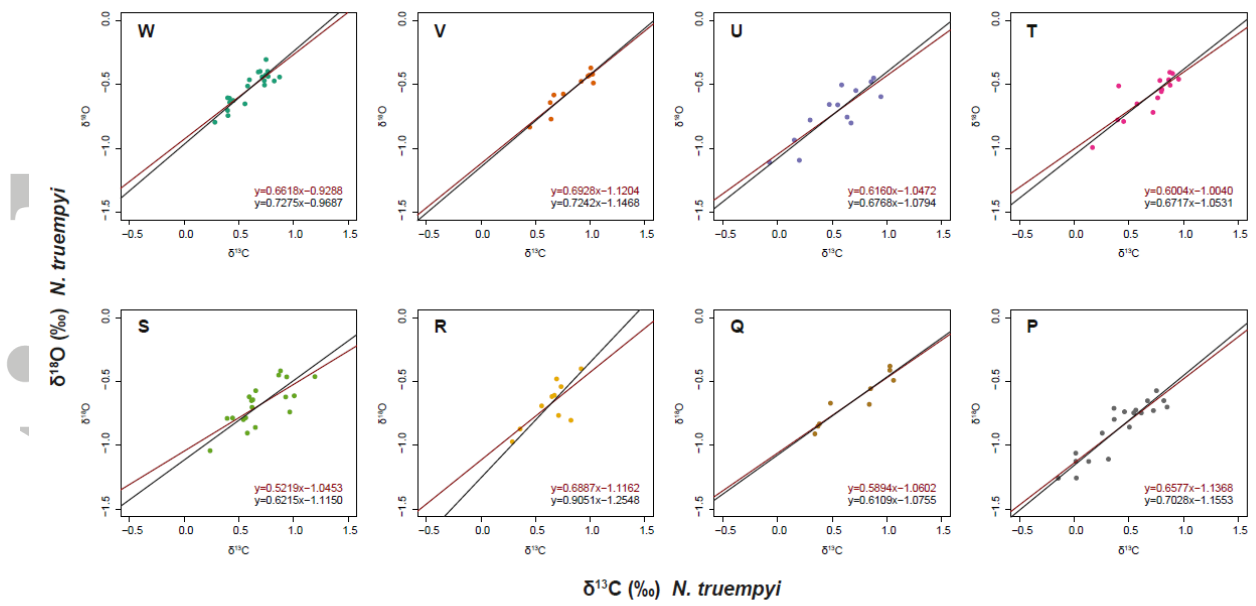


Figure 6. Covariance between $\delta^{13}\text{C}$ and $\delta^{18}\text{O}$ for the younger hyperthermal events (P to W) using linear (red) and Deming (black) regression. For all the events, changes in the exogenic carbon pool are linearly related to warming.

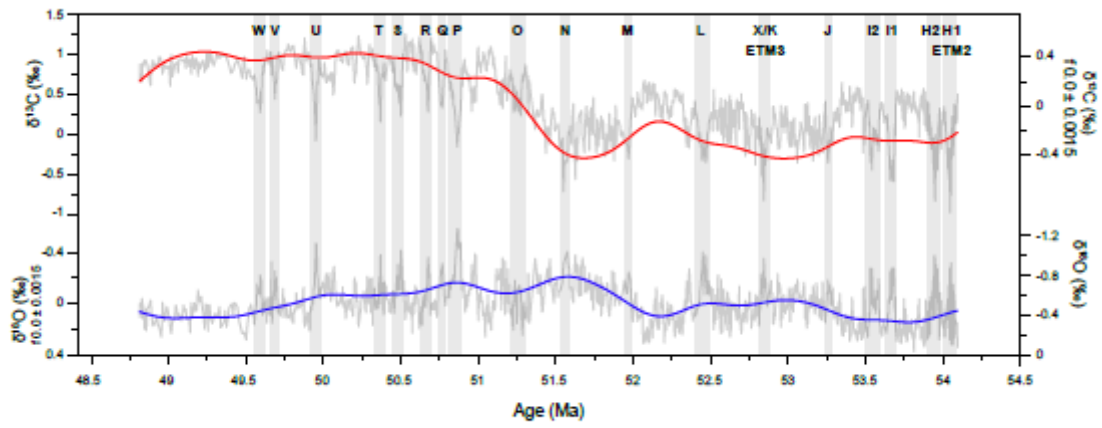


Figure 7. Long term trends extracted from the for $\delta^{13}\text{C}$ and $\delta^{18}\text{O}$ benthic records by applying Gaussian filtering ($f. = 0$; bandwidth = 0.0015).

Accepted Article